www.czasopisma.pan.pl PAN www.journals.pan.pl
Opto-Electronics Review 27 (2019) 79–89

Contents lists available at ScienceDirect

Opto-Electronics Review

journal homepage: http://www.journals.elsevier.com/opto-electronics review

Modelling of a two-dimensional photonic crystal as an antireflection coating for optoelectronic applications

D. Przybylski*, S. Patela

Faculty of Microsystem Electronics and Photonics, Wroclaw University of Science and Technology, 11/17 Janiszewskiego St., 50-372 Wrocław, Poland

ARTICLE INFO

Article history:
Received 2 October 2018
Received in revised form 11 February 2019
Accepted 13 February 2019
Available online 19 March 2019

Keywords:
Photonic crystal
Modelling
FDTD method
Antireflection
Coating

ABSTRACT

In article a two-dimensional photonic crystal (PhC) is considered and modelled as a new generation antireflection coating for optoelectronic devices. Traditional antireflective coatings (ARCs) reduce the reflection of the radiation only – the new generation of antireflective coatings should affect the distribution of the radiation also. Such functionality can be provided by the two-dimensional PhC which reduce the reflection and scatter transmitted light. Prior to the fabrication, the PhCs should be designed and analysed. Results of the analysis should provide quantitative means for choice of materials and design solutions. In work, we analyse the electromagnetic field distribution as Poynting vectors inside the materials of optoelectronic devices, in order to investigate the possibility of improving the construction of future optoelectronic devices. Furthermore, we calculate the reflection and transmission of that ARC. It's a complex optic analysis of new generation of ARC. The numerical analysis has been performed with the FDTD method in Lumerical Software. In work, we consider the two-dimensional photonic crystal on the top surface of optoelectronic structures. We compared the results with the traditional ARC from these same parameters as PhC: thickness and material. As an example, we presented the application of modelled, photonic crystal, thin-film, GaAs solar cells with PhC on top. The efficiency of this solar cell, using the photonic crystal, was improved by 6.3% over the efficiency of this same solar cell without PhC. Thus, our research strongly suggests that the unique properties of the photonic crystal could be used as a new generation of ARC.

1. Introduction

1.1. Introduction to a new generation of antireflection coating

The purpose of using antireflection coatings (ARCs) is to increase the amount of radiation reaching the optoelectronic structure [1] by reducing the reflection from the surface. The antireflection coatings are fabricated from different materials, depending on the substrate selection, technology and operational requirements. There are several ways to reduce reflection from the device surface. The most common is a single or multilayer coating [2]. For a reduction in reflection [3], as well as texturization of the top surface of the [4] including surface textures [5] or a [6]. The traditional antireflection coatings simply change the amount of the radiation reaching the active part of a photonic device. However, from a point of view of device designer, it would be desirable to controll [7]. The new ARCs change the length of paths of optical beams that travel through optoelectronic devices. Moreover, those structures can create a light-trapping effect. In this light-trap, the photons may have a path several times longer than the actual thickness of the device and can be absorbed in very thin layers [8]. The idea of traditional and new generation antireflection coatings is presented in Fig. 1.

Photonic crystals (PhC) and their optical properties have attracted much attention in the last quarter-century [9]. They are used in different applications, e.g. detectors and photovoltaic cells [7]. In particular, photonic crystals are useful for light trapping because changing parameters of the PhC changes the transmission and reflection of the incident radiation [7].

Already the one-dimensional PhCs are applied as a distributed Bragg reflector (DBR) [10]. In Ref. 10, the improvement of the efficiency of an c-Si solar cell was increased to approx. 20% after using the PhC. In Ref. 11, the efficiency of an a-Si solar cell increased by approx. 2% in comparison to the structure without PhC. The transmission of antireflection coating increased by 5% when the PhC was used as a smart window for low-temperature applications [12]. In Ref. 13 the efficiency of a c-Si solar cell increased by approx. 5.5% after the two-dimensional photonic crystals are used as a back reflector. In Ref. 14 the PhC was used in thermophotovoltaic applications and the absorption increased to 32% when the PhC was used as ARC layer.

* Corresponding author.
E-mail address: dariusz.przybylski@pwr.edu.pl (D. Przybylski).

https://doi.org/10.1016/j.opelre.2019.02.004
1230-3402/

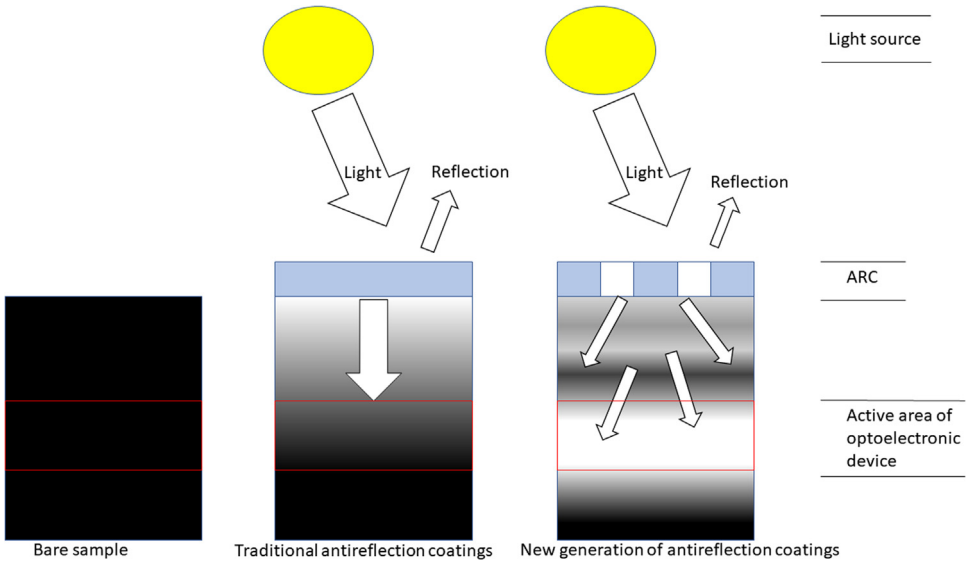

Fig. 1. The idea of traditional and new generation of ARCs: The bare (uncoated) sample is unlighted so the radiation does not appear inside of the structure. For traditional ARC, the light reaches the structure, but the radiation is not deflected. The new generation of ARC reduces the reflection, as do a traditional ARC, but deflect the light and adjust the distribution of electromagnetic field with the active area of an optoelectronic device.

So far, the literature has shown how to use the PhCs to improve parameters of optoelectronic devices [15–18] in specific structures and for selected combination of materials. However, a comparative analysis of the electromagnetic field distribution and transmission characteristics for different material compositions was not provided. In Refs. 19–21 articles, authors have calculated the energy field distribution inside the structures, but they have not considered the transmission and reflection of analysed devices. Ref. [22] considered modelling of PhC as an antireflection coating. However, authors have not analysed the energy distribution inside the optoelectronic structure. In Ref. 23, authors have performed complex optical analysis of reflection and transmission of photonic crystal's structure and energy field distribution inside the device. However, it was calculated and considered only for organic material.

In this paper, we present a detailed analysis of using the PhC for improving efficiencies of optoelectronic structures. Poynting vector distribution, transmission, reflection and absorption are calculated and compared for different substrates and different PhC materials. To our knowledge, it was not done previously.

1.2. Introduction to modelling of photonic crystals

Modelling of the PhC performance is done with the methods used for calculation of electromagnetic field propagation and distribution [24]. The most popular methods are the plane wave expansion method (PWE) and finite-difference time-domain (FDTD) [24,25]. The PWE method is adequate for the planar and homogeneous structures [26]. However, this method does not provide information about distribution of optical power inside the optoelectronic devices [27]. The FDTD method is more universal and is capable of analysis of heterogenous structures with rapidly changing topological details [28].

The FDTD method divides the area of interest into small calculation cells, with the cell dimensions usually ranging from a few to several tens of nanometers [28]. For efficient modelling the number of cells should be kept as low as possible. For this reason, in the numerical analysis, only part of the structure is selected where the interactions that are of interest take place. On the edges of that region numerical boundary conditions are placed. The traditional boundary conditions are those which have to be fulfilled for fundamental physical reasons, at the boundaries of the devices, while solving the relevant equations [29]. On the other hand the numerical boundary conditions provide the information for the algorithm about the behaviour of the electromagnetic field at the edges of the modelling area [28].

FDTD models of the PhCs yield information about reflection, transmission and the optical band structure [24]. Furthermore, with the FDTD method, the Poynting vector distribution and the information about scattered radiation inside the optoelectronic device can be calculated. This information is important for optimizing detectors and solar cells in a thin-film technology [30]. The analysis of the field distribution shows the regions of high intensity of radiation formed within the structure. In these areas the active parts of semiconductor devices, e.g., p-n junctions of photodetectors, should be located [30,31].

2. Modelling of the photonic crystal

2.1. Details of the modelling process

In this work we have modelled a two-dimensional PhC with the finite-difference-time-domain (FDTD) using the Lumerical FDTD software. For the modelling work we have selected gallium arsenide (GaAs) and silicon (Si), the popular photonic materials [32]. These materials served as substrates for both PhCs and traditional one-layer antireflection coatings (ARC) (Fig. 1). Semiconductor devices are typically manufactured on substrates with a thickness ranging from a few micrometers up to several hundred micrometers. For our modelling we assumed the modeling area to be 2 μm thick, as this is a typical value for a p-n junction in thin-film optoelectronic devices [31]. With this value we analysed the influence of PhC and traditional, single-layer antireflection coating on the electromagnetic field distribution below the surface of potential optoelectronic devices. The operation of PhCs strongly depends on the refractive index of materials from which they are built [25]. For our modelling we have selected two materials of significantly different refractive indices: high-refractive-index aluminium oxide (Al_2O_3, $n_{Al2O3} \approx 1.76$) and low refractive index polymer (polymethyl methacrylate PMMA, $n_{PMMA} \approx 1.49$) [33].

Refractive indices of the materials were taken from Palik [34] and [33]. As a light-source spectrum, we adopted the AM 1.5 solar spectrum generated by the Lumerical program. The simulations

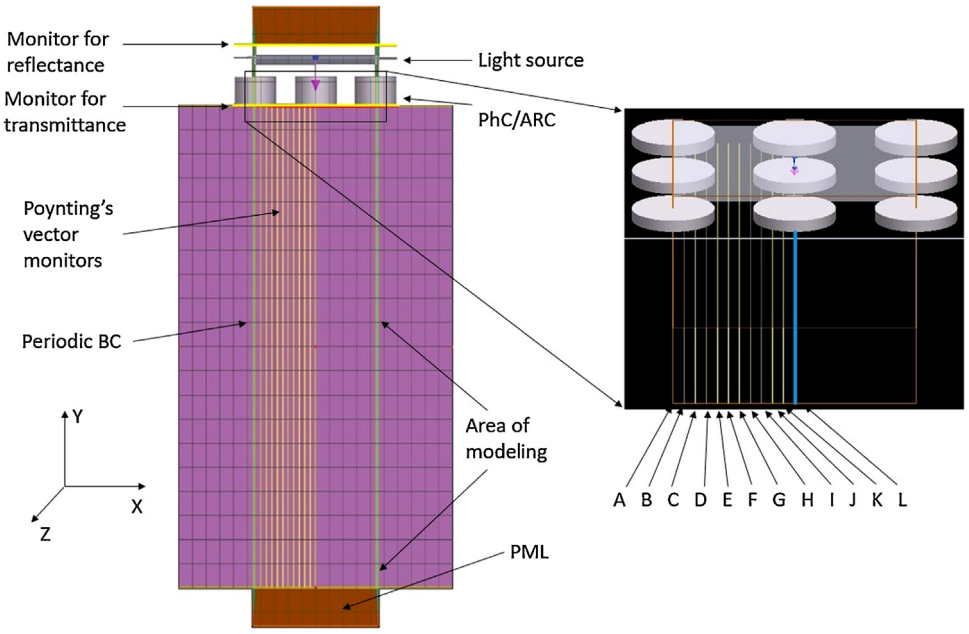

Fig. 2. Schematic of the modelling region. The parameters are measured by the monitors, which take form of planes, limited by the area of modelling. YZ-plane monitors control the Poynting vector, and XZ monitors control transmission and reflection. The inset on the right shows the locations of 12 Poynting monitors, marked A to L.

were carried out in the spectral range from 300 nm to 1100 nm, as this range covers the most significant range of the AM 1.5 solar spectrum. Furthermore, the optoelectronic devices made of silicon or GaAs, often work in this range [31]. The angle of incidence was set to 0 degrees and was not changed during the modelling process. The modelled area is marked by the green rectangle in Fig. 2, with the following dimensions: Y from 0 to 2.3 μm, X and Z: from − 0.44 to 0.44 μm. The orientation of the axis is shown in Fig. 2.

We selected transmittance, reflectance and Poynting's vector as parameters describing the performance of analysed structures. In the Lumerical software used, the parameters are established with the help of so-called "monitors." Frequency-domain field monitors collect the field profile in the frequency domain from simulation results across a spatial region within the simulation in the FDTD [35]. The group of Poynting's monitors from Fig. 2 were set up as plane monitors set at several X coordinates (Y: 0 – 2 μm, Z: −0.44 to 0.44 μm, X: set position), which allowed us to obtain information about the direction of power flow in 3D. As shown in Fig. 2 each monitor is marked by a letter and can be addressed and positioned individually.

2.2. Calculation mesh and numerical boundary conditions

The numerical analysis of the electromagnetic field behaviour inside photonic devices start with the selection of a set of equations defining physical prerequisites and the numerical method. Working within the established modelling environment, the user has to make choices according to the scope of research, available computational power and required accuracy of the analysis.

If the FTDT method is applied, the calculation cell size has to be defined. The size of the cell can be specified in units of length or in a relative way, in reference to the wavelength. For our calculations the mesh of was set to 16 ppw (points per wavelength) to ensure a modelling error of 0,01%. 16 ppw meant that the mesh cell size was:

$$g = \frac{\lambda}{16 \cdot n(\lambda)} \quad (1)$$

where:

g is the size of simple Yee's cell [28] for a given wavelength,

λ is the wavelength,

n(λ) is the dispersion of the material.

Particularly, in the case of our modelling process, the mesh cells size ranged from 3.8 nm (wavelength of 300 nm) to 19.4 nm (wavelength of 1100 nm) for Si and from 5.0 nm (wavelength 300 nm) to 19.9 nm (wavelength of 1100 nm) for GaAs.

2.3. Selection of numerical boundary conditions

The boundary conditions are the necessary component of the analysis of photonic devices with differential equations - they define the shape of the analyzed structure and its constraints. In numerical modelling another set of numerical conditions is required: the so-called numerical boundary conditions. The numerical boundary conditions set the limits of the modelling area (which is usually different from device boundaries) and control the behaviour of electromagnetic field at these limits.

The perfectly matched layer (PML) is the artificial absorbing boundaries for wave equations. The PML is usually used to truncate the analysis and region of the simulations [36]. The PML boundary numerically absorbs the light and eliminates reflections (ideal PML provide zero reflection) [37].

Lumerical FDTD uses the new formulation of PML based on the stretched coordinate formulation [38], where the users can directly specify all the parameters that control the absorption properties of the selected PML boundaries [39]. The user can also select PML profiles and fine tune the number of layers. For our modelling, we have selected a standard profile of PML. The number of PML layers was set to 20.

The Periodic and Bloch boundary conditions are used in the case of periodic structures [40,41]. These boundary conditions cause that the area of the simulation can be minimized to simply periodically recurrent cells. In our simulation different numerical boundary conditions are selected for different directions. Numerical boundary conditions used by us are listed in Table 1.

The 3D simulations have been used for modelling photonic-crystal-based AR coatings, uncoated structures, and standard AR coatings.

Table 1
The boundary conditions used by un in the modelling of two-dimensional PhC as an antireflection coating for optoelectronic applications.

Direction	Axis X	Axis Z	Axis Y
Boundary condition	Periodic BC		PML

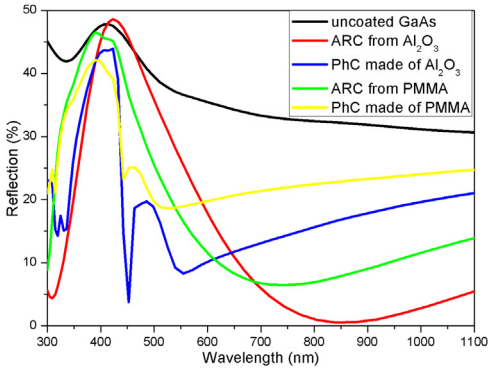

Fig. 3. Reflectance as a function of wavelength for PhCs and thin film ARC made of PMMA and Al_2O_3, deposited on top of the GaAs substrate. Reflectance of an uncoated GaAs is also given for the reference.

2.4. Modelling of antireflection coatings

We investigated a two-dimensional PhC deposited on the top of the GaAs and Si substrates. For numerical analysis, a 2 μm topmost layer of the substrate was selected. The PhC was formed by nanocylinders of aluminium oxide or PMMA. Aluminium oxide was selected, as the value of its refractive index, approximately equal to a square root of the refractive index of gallium arsenide, makes it a natural choice for ARC [42]. PMMA was chosen for its popularity and ease of processing [43,44].

The following parameters of the PhC were set after the previous optimization [45]: lattice constant a = 440 nm, the diameter of nanocylinders Φ = 300 nm and layer thickness (the height of nanocylinders) d = 120 nm.

The PhCs were compared with traditional (plain layer) ARCs from PMMA and aluminium oxide, deposited on the top of the analysed substrates. The thickness of ARCs was set to 120 nm, which is the same value as the height of nanocylinders in PhC's antireflection structures. We selected reflectance, transmittance, Poynting vector and optical generation as quantitative results of the analysis. As a reference for the achieved reflection results the uncoated substrate of gallium arsenide and silicon was used. For calculations of the transmission the 120 nm thin films of Si and GaAs were used as a reference.

2.4.1. Results of the modelling process of antireflection coatings

In this chapter calculated results of reflectance and transmittance are presented. Results were obtained according to the procedures described in chapters 2.1 and 2.2, and registered by the monitors indicated in Fig. 2. In the calculations, the photonic crystal and traditional ARC were considered for gallium arsenide and silicon substrates.

In Fig. 3 reflectance of ARCs deposited on the GaAs substrate is shown. There are two PhC coatings and two plain layer coating, both made of Al_2O_3 and PMMA. There is also reflectance curve from the uncoated GaAs provided for the reference.

In the 300–1100 nm spectral range reflectance from the uncoated substrate of gallium arsenide is the same as a literature reference [34], which verifies correctness of the selected numerical procedure. All types of the analysed ARCs reduce the reflection from the surface of gallium arsenide. In the visible range,

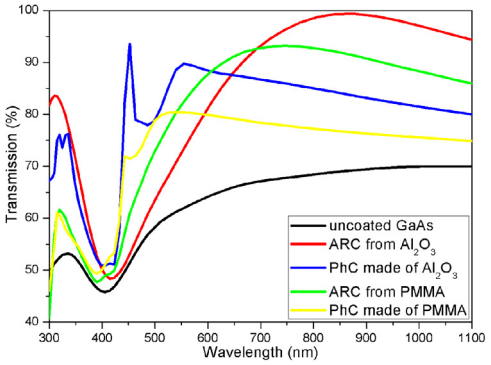

Fig. 4. Transmission as a function of wavelength for PhCs and thin film ARC made of PMMA and Al_2O_3, deposited on top of the GaAs substrate. Transmission of an uncoated GaAs surface is also given for the reference.

the Al_2O_3 PhC coating reduces the reflection better than the plain layer ARC. For the PMMA material that effect is observed in the range from 320 nm to 550 nm. In the remaining part of the spectrum plain layer of PMMA works better than PhC-film. In the near infrared, both traditional ARCs reflect less radiation than PhC's coatings. The PhC's coatings exhibit fluctuations in the visible range of light.

In Fig. 4. transmission of ARCs deposited on the GaAs substrate is shown. As previously, there are two curves for PhC coatings and two plain layer coating, both made of Al_2O_3 and PMMA. There is also a reference curve from the uncoated GaAs.

Comparing reflection and transmission characteristics of ARCs made of Al_2O_3 and PMMA we notice, that the coating of the material with higher refractive index allows more radiation into the substrate. The same observation is true for PhCs. The PhC, made of the material with higher value of refractive index introduces more radiation into the optoelectronic structure. However, higher contrast of refractive index between the nanocylinders and their surroundings (in this case it is air) is important for PhCs. The effects from the wave optics have the influence on the shape of the transmission characteristics of PhC. For this reason, the analyse of PhC as new generation antireflection coating is unintuitive and requires a lot of calculation.

Comparing the curves from Figs. 3 and 4 we can say that Al_2O_3-PhC is better than PMMA-PhC, as more radiation will reach the structures within the GaAs substrate. Assuming that transmission, reflection, and absorption are related by the equation [46]:

$$1 = R + T + A, \tag{2}$$

where:
R is the reflection,
T is the transmission,
A is the absorption,
absorption has been calculated. The results are presented in Figs. 5 and 8.

The coatings of PMMA absorb strongly the radiation in the range from ultraviolet to approx. 320 nm. Out of this range, the absorption of PMMA decreases.

In Fig. 6. the reflectance of ARCs deposited on Si substrates is shown. There are two PhC coatings and two plain layer coatings, both made of Al_2O_3 and PMMA. There is also a reflectance curve from the uncoated Si provided for the reference. In the 300–1100 nm range we obtained the same result of simulated reflectance for uncoated samples from silicon as literature reference [34] which, again, verifies correctness of the numerical procedure.

The plain-layer ARC from Al_2O_3in the range from 400 nm to 480 nm exhibits the reflection higher than that for the uncoated

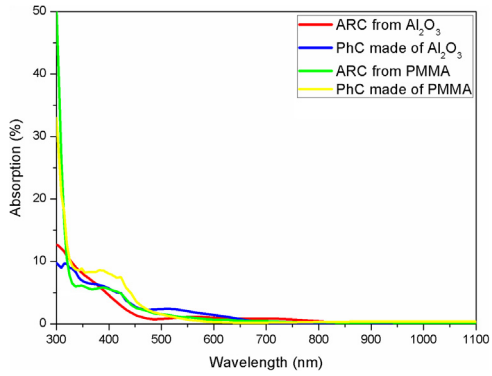

Fig. 5. Absorption as a function of wavelength for PhC ARC made of PMMA and Al_2O_3, deposited on top of GaAs substrate.

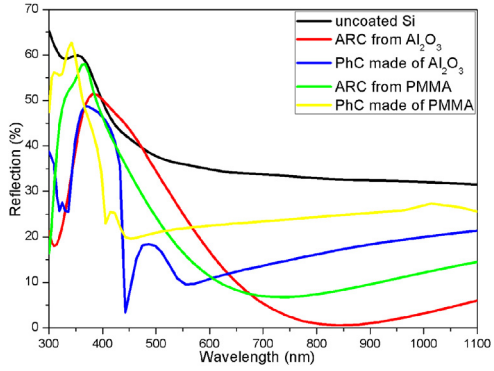

Fig. 6. Reflectance as a function of wavelength for PhjC ARC made of PMMA and Al_2O_3, deposited on top of the Si substrate. Reflectance of an uncoated Si is also given for the reference.

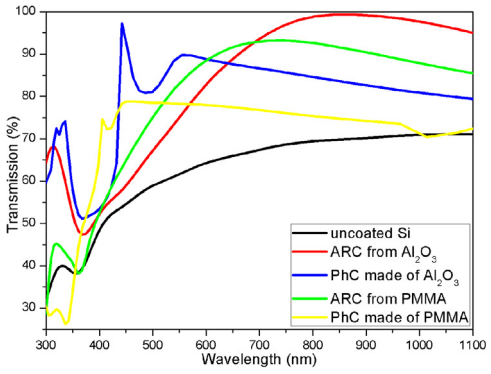

Fig. 7. Transmission as a function of wavelength for photonic-crystal made of PMMA and Al_2O_3, deposited on the top of the Si. Transmission of an uncoated Si is also given for the reference.

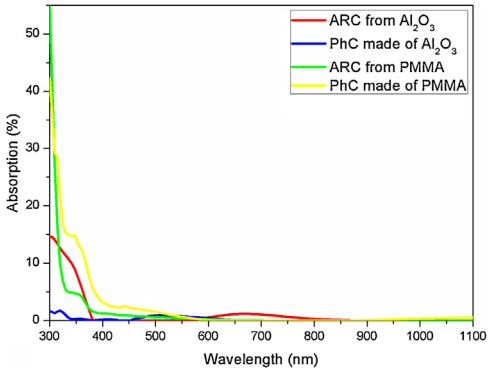

Fig. 8. Absorption as a function of wavelength for PhC made of PMMA and Al_2O_3, deposited on the top of the Si substrate.

Si. For Al_2O_3 material one can see that PhC in the spectral range from 350 nm to 650 nm reflects less radiation than ARC in the same range. However, for range from 650 nm to 1100 nm, ARC has lower reflectance than PhC.

The PhC made of PMMA have changed the reflection of light but, in the range from 340 nm to 360 nm, the reflection was worse than that for the uncoated Si. For PMMA's material one can see that PhC in the spectral range from 370 to 520 nm reflects less radiation than ARC in the same range. Out of this range, the ARC from PMMA has the smallest reflectance than for PhC.

The reflectance data from Fig. 6. show that only PhC made of Al_2O_3 and ARC from PMMA reduced the reflection in the whole analysed spectral range. The reflection for the PhC made of Al_2O_3 reduced the reflection most.

Figure 7 shows that the best transmission is obtained for PhC and ARC made of Al_2O_3.

The PMMA absorbs most of the radiation from 300 nm to 350 nm. Out of the range, the absorption of PMMA decreases. It was expected that the same result of absorption for coats from PMMA on the Si is like for coats from PMMA on the GaAs. The PhCs introduce some different transmission in the range from 300 nm to 400 nm. Probably, it is caused the construction and effects of PhCs.

Transmission, absorption and reflection at the surface help us to select the AR layer. However, we don't receive the information about the propagation and distribution of radiation underneath the ARC and PhC. The quantitative information is obtained by calculating and analysing energy flow and field distribution inside the studied structures, which is done in the following chapter.

2.5. Optical energy distribution

In this chapter, we present the result of the calculation of the electromagnetic energy distribution within the optoelectronic structure. The energy is calculated as the Poynting vector [47] distribution within the substrate. The Poynting vector has been calculated for 700 nm wavelength. For this wavelength, both optoelectronic materials absorb the light. Moreover, this is the centre wavelength of the analyse spectrum.

For the analyzis we have selected the region where for a p-n junction of optoelectronic devices are usually located [31]. The Poynting vector gives us information both about the distribution and direction of the energy flow. The results of the Poynting vectors analysis are presented as the cross sections (Fig. 2) of the optoelectronic structure. The Poynting vector is calculated only for radiation inside the optoelectronic structure. All of the obtained results were presented on the figures in the range of coloured scale from 0 to 3 $\frac{mW}{m^2}$.

We show the way of analysis of the influence of the PhCs and traditional ARCs on the transmitted light inside the devices. Therefore, the Poynting vectors are not presented and calculated inside the PhCs and ARCs.

Figures 9 and 10 show Poynting vectors inside the optoelectronic device for PhC made of Al_2O_3 and PMMA deposited on the top of the GaAs structure. The difference between power density to PhCs from other materials is of approximately 0.3 $\frac{mW}{m^2}$ for the beginning of the optoelectronic structure. This value has been read from data on the centre of Poynting vectors F and G. Moreover, approximately the same value is for the same point of Poynting vector, but for different ARCs for the same substrate (e.g., Poynting vector F from Figs. 9 and 10).

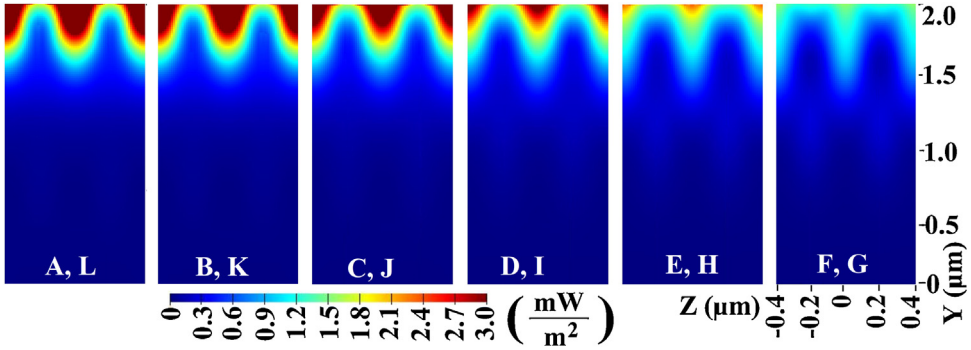

Fig. 9. Poynting vectors (control by YZ-plane monitors marked A to L in Fig.2) as the electromagnetic field distribution (is symmetric, the results from A–F to G–L YZ-plane monitors are identical, so we presented only half of monitors) at 700 nm wavelength, inside the GaAs substrate after passes through the PhC made of aluminium oxide, deposited on the top of the structure.

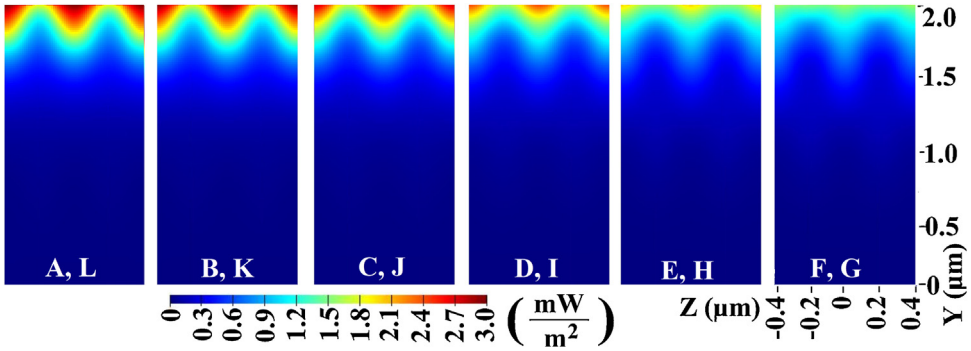

Fig. 10. Poynting vectors (control by YZ-plane monitors marked A to L in Fig.2) as the electromagnetic field distribution (is symmetric, the results from A–F to G–L YZ-plane monitors are identical, so we presented only half of monitors) at 700 nm wavelength, inside the GaAs substrate after passes through the PhC made of PMMA, deposited on the top of the structure.

More of radiation reach the inside of the GaAs structure for a PhC made of aluminium oxide.

Compared to classical ARC, PhCs have an additional property to deflect radiation like diffraction grating. That property is important to thin-film photonic devices [7]. Forasmuch, the optical path is longer and the wavelengths have more chance to be absorbed by the optoelectronic device.

The FDTD method summarizes all of the wave optics effect. Therefore, the origin of the energy field distribution is a group of results: resonances in subsequent cylinders, diffraction and other wave optics effect.

In Figs. 9 and 10 this property is observed as the perturbation of power flow on the different depth of the optoelectronic structures. In the case of PhC made of Al_2O_3 the perturbation of power flow is depth than for PhC made of PMMA. Moreover, analysing the data from Figs. 9 and 10, PhC made of Al_2O_3 deflect the radiation more than PhC made of PMMA.

Figures 11 and 12 show Poynting vectors for PhC made of Al_2O_3 and PMMA deposited on top of the Si structure.

Analysing the data from Figs. 11 and 12 we see that both PhCs deflect radiation in a similar way. However the difference between power density for this PhC from different materials is of approximately 0.3 $\frac{mW}{m^2}$. That difference in the value of power density, less reflection and better transmission of radiation show that for the Si substrate, PhC made of Al_2O_3 is better.

To verify optical properties of PhCs we have compared them with one-layer antireflection coatings from the same materials and thickness as the considered PhCs.

Figure 13 shows Poynting vectors inside the GaAs substrate for an uncoated sample of gallium arsenide and ARCs from different materials.

Looking at Poynting vectors inside the GaAs substrate for an uncoated sample of GaAs and for ARC deposited on the top of the structure, we see that power fades exponentially inside the structure.

There is no power change for the Z direction, which means that the light wasn't deflected. The values of power density show that ARC made of Al_2O_3 allows for more radiation inside the structure than ARC made of PMMA. The difference between that ARCs is of approximately 0.25 $\frac{mW}{m^2}$. The difference is less than that between PhCs from different materials.

Figure 14 shows Poynting vectors inside the Si substrate for an uncoated sample of silicon and ARCs made of different materials, deposited on the top of the silicon structure.

Analysing Poynting vectors inside the Si substrate for an uncoated sample of Si and ARCs, deposited on the top of Si structure, shows that power decays inside the structure. There is no decay for the Z direction, which means that the light is not deflected. The values of power density show that ARC from Al_2O_3 introduces more radiation to the structure than ARC from PMMA. The difference between those ARCs is of approximately 0.3 $\frac{mW}{m^2}$. The difference is bigger than for PhCs made of different materials and materials deposited on the Si substrate.

The Poynting vectors provide information about the electromagnetic field distribution inside the substrates. However, the Poynting vectors present the results only for the single wavelength. For this reason, we introduce the optical generation as the parameter which is took into account the materials properties and their impact on the whole analysed spectrum.

However, it is not related to the properties of the material used. For this reason, we have calculated the optical generation parameter which facilitate the design process of optoelectronic devices.

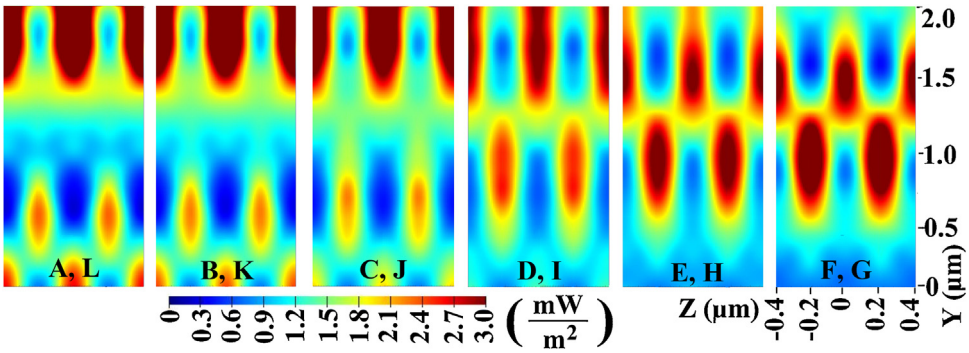

Fig. 11. Poynting vectors (control by YZ-plane monitors marked A to L in Fig.2) as electromagnetic field distribution (is symmetric, the results from A–F to G–L YZ-plane monitors are identical, so we presented only half of monitors) at 700 nm wavelength, inside the Si substrate after passes through the PhC made of aluminium oxide, deposited on the top of the structure.

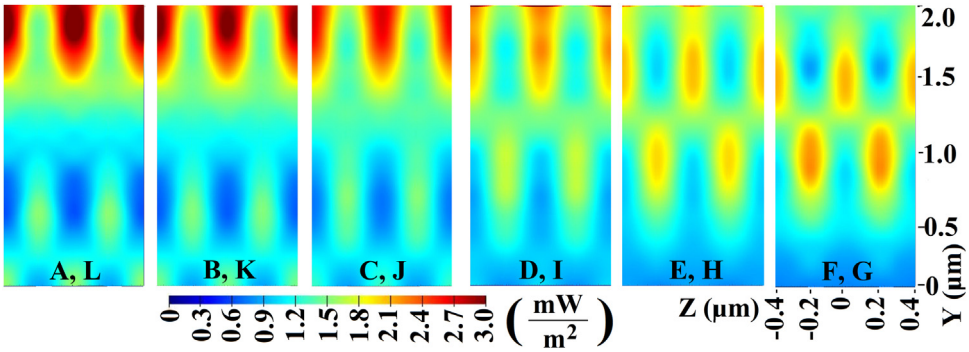

Fig. 12. Poynting vectors (control by YZ-plane monitors marked A to L in Fig.2) as electromagnetic field distribution (is symmetric, the results from A–F to G–L YZ-plane monitors are identical, so we presented only half of monitors) at 700 nm wavelength, inside the Si substrate after passes through the PhC made of PMMA, deposited on the top of the structure.

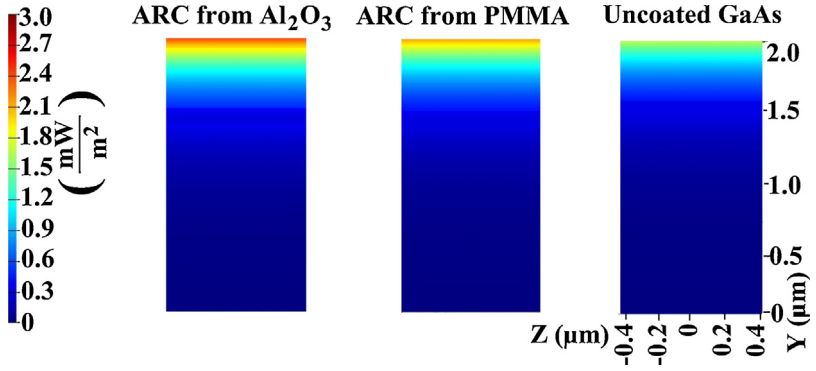

Fig. 13. Poynting vectors (control by YZ-plane monitors marked A to L in Fig. 2) as electromagnetic field distribution (is symmetric, the results from A–F to G–L YZ-plane monitors are identical, so we presented only half of monitors) at 700 nm wavelength, inside the GaAs substrate after passes through ARCs deposited on the top of the structure and uncoated GaAs.

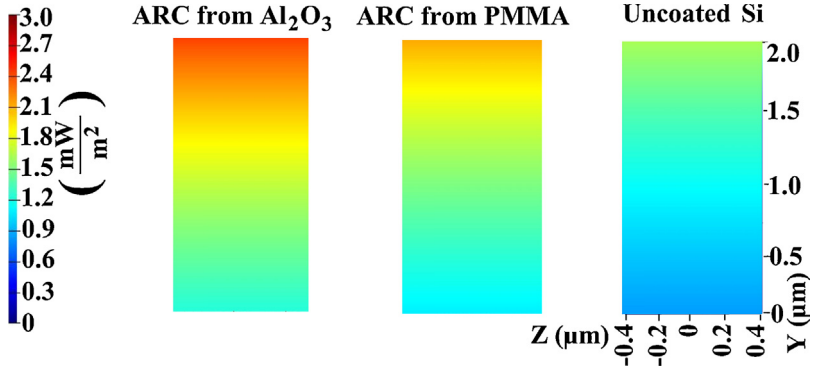

Fig. 14. Poynting vectors (control by YZ-plane monitors marked A to L in Fig. 2) as electromagnetic field distribution (is symmetric, the results from A–F to G–L YZ-plane monitors are identical, so we presented only half of monitors) at 700 nm wavelength, inside the Si substrate after passes through ARCs deposited on the top of the structure and uncoated Si.

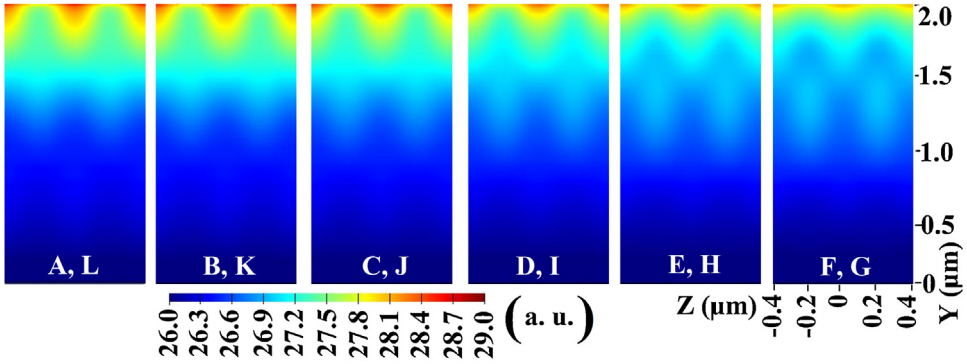

Fig. 15. Optical generation (calculated for YZ-plane monitors marked A to L in Fig. 2) in analysed spectrum (the results are symmetric from A–F to G–L YZ-plane monitors, so we presented only half of monitors), inside the GaAs substrate after passes through PhC made of aluminium oxide, deposited on the top of the structure.

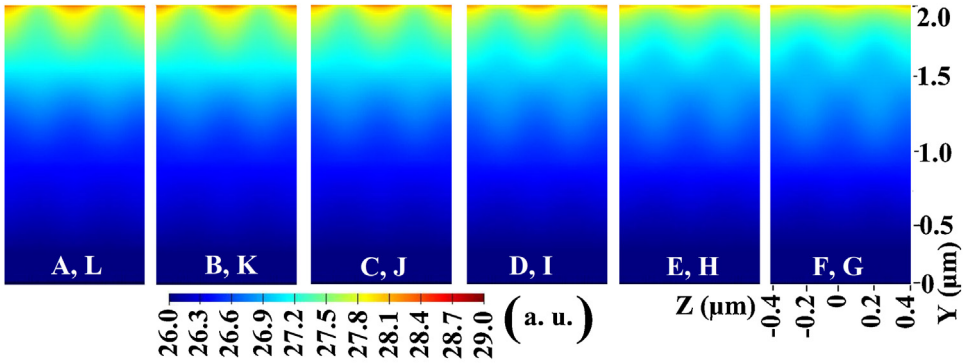

Fig. 16. Optical generation (calculated for YZ-plane monitors marked A to L in Fig. 2) in analysed spectrum (the results are symmetric from A–F to G–L YZ-plane monitors, so we presented only half of monitors), inside the GaAs substrate after passes through PhC made of PMMA, deposited on the top of the structure.

2.6. Optical generation

The "optical generation" is the parameter calculated by the Lumerical-FDTD software to characterize response of the material to light. It represents the number of carriers generated inside the illuminated structure. The calculations of the optical generation have been performed for the same monitors' locations as the calculation of Poynting vectors (Fig. 2). For clarity of comparison of the results between different cases of substrates and antireflection coats, the optical generation functions were presented on a logarithmic scale:

$$f\left(G_{opt}\right) = log_{10}G_{opt}, \tag{3}$$

where:

G_{opt} is the the optical generation.

In the real case the values of the optical generations were from $1{\cdot}10^{26}\ \frac{1}{cm^3}$ (on the scale 26.0 a.u.) to $1{\cdot}10^{29}\ \frac{1}{cm^3}$ (on the scale 29.0 a.u.).

Figures 15 and 16 show optical generation for PhC made of Al_2O_3 and PMMA deposited on top of the gallium arsenide structure.

The origins of optical generation presented in Figs. 15 and 16 are similar to the origins of Poynting vectors showed in Figs. 9 and 10. In comparison to the Poynting vectors, presented only for one wavelength (chapter 2.4), the optical generation included results for all analysed spectrum (AM 1.5). It confirms that, the minimums and maximums of electromagnetic field distribution are the mapping of generated carriers in the illuminated structure. It means, that calculation of Poynting vector for only one wavelength is enough to define the area with increased number of generated carriers in the illuminated structures.

Figures 17 and 18 present optical generation for PhC made of Al_2O_3 and PMMA deposited on top of the Si structure.

The origins of the optical generations, showed in Figs. 17 and 18, conform the origins of Poynting vectors presented in Figs. 11 and 12. The same relation of origins was observed also for the GaAs substrate with PhC made of different materials.

Figure 19 shows optical generation inside the GaAs substrate for an uncoated sample of gallium arsenide and ARCs from different materials.

The exponential shape of function of optical generations, for the GaAs substrate with ARCs deposited on top of structure and uncoated GaAs, conform also the shape of function of Poynting vectors (Fig. 13).

Figure 20 shows optical generation inside the Si substrate for an uncoated sample of silicon and ARCs made of different materials, deposited on the top of the silicon structure.

Analysing the data from Fig. 20, we noticed the same relation of the origins and they conform with Poynting vectors (Fig. 14).

To receive the useful information in creating the optoelectronic devices, the optical generations were summarized. The substrates were divided in three areas: the top: from 2 to 1.5 μm, the centre: from 1.5 to 0.5 μm and the bottom: from 0.5 to 0 μm. In divided areas, the optical generations were summarized and the results were presented in Table 2. The percentages values were calculated in comparison to uncoated substrate with the same geometry volume.

The data presented in Table 2 confirmed that the PhC allows to generate six-eightfold more carriers than uncoated structure and substrate with traditional ARC deposited on the top structure. The three areas can help to define the position of the active region of creating optoelectronic device according applied PhC or ARC from PMMA or Al_2O_3 deposited on the top of GaAs or Si substrate. The material for ARC and PhC with high contrast of refractive index to

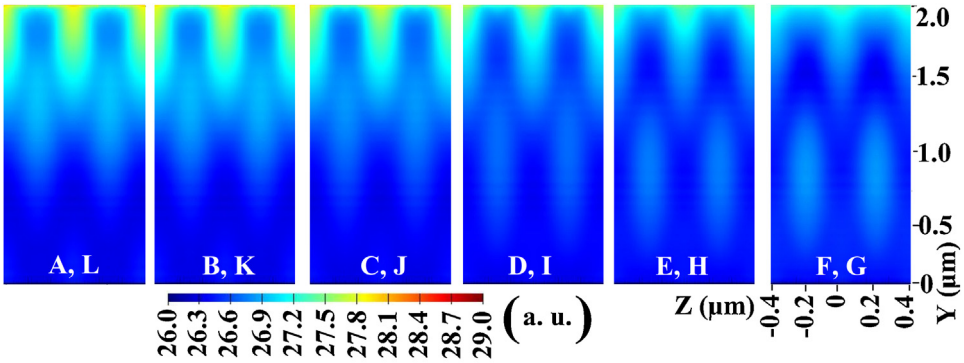

Fig. 17. Optical generation (calculated for YZ-plane monitors marked A to L in Fig. 2) in analysed spectrum (the results are symmetric from A–F to G–L YZ-plane monitors, so we presented only half of monitors), inside the Si substrate after passes through PhC made of aluminium oxide, deposited on the top of the structure.

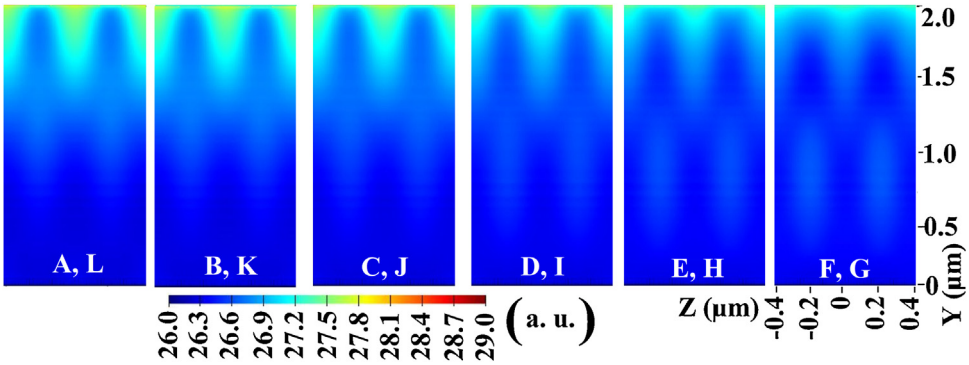

Fig. 18. Optical generation (calculated for YZ-plane monitors marked A to L in Fig. 2) in analysed spectrum (the results are symmetric from A–F to G–L YZ-plane monitors, so we presented only half of monitors), inside the Si substrate after passes through PhC made of PMMA, deposited on the top of the structure.

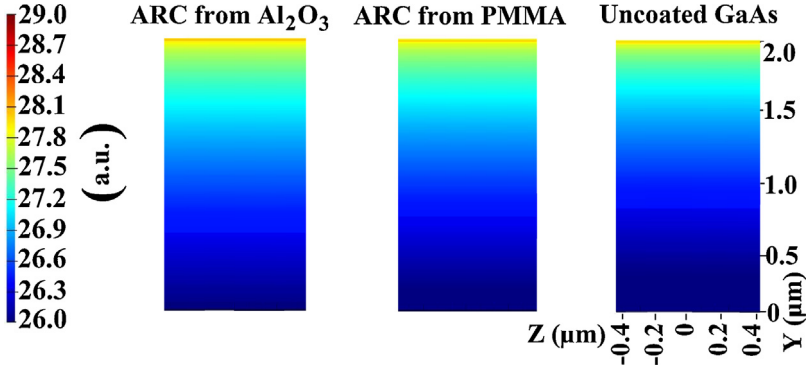

Fig. 19. Optical generation (calculated for YZ-plane monitors marked A to L in Fig. 2) in analysed spectrum (the results are symmetric from A–F to G–L YZ-plane monitors, so we presented only half of monitors), inside the GaAs substrate after passes through ARCs deposited on the top of the structure and uncoated GaAs.

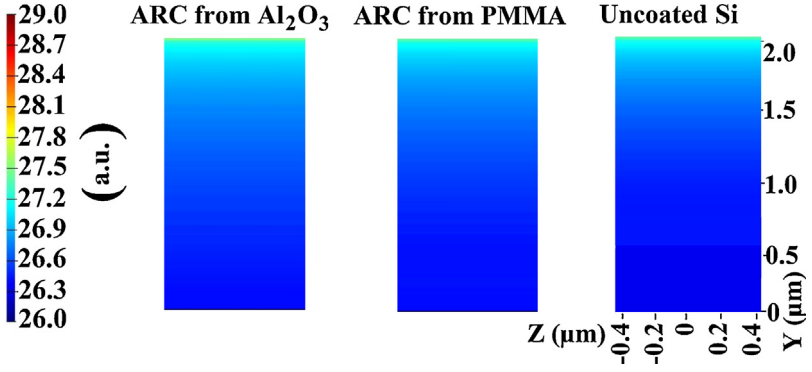

Fig. 20. Optical generation (calculated for YZ-plane monitors marked A to L in Fig. 2) in the whole analysed spectrum (the results are symmetric from A–F to G–L YZ-plane monitors, so we presented only half of monitors), inside the Si substrate after passes through ARCs deposited on the top of the structure and uncoated Si.

Table 2
The summary of the optical generation in three areas for different substrates, PhCs and ARCs.

Substrate	Area	ARC				PhC			
		PMMA		Al_2O_3		PMMA		Al_2O_3	
		[%]	$\left[\frac{1}{cm^3}\right]$	[%]	$\left[\frac{1}{cm^3}\right]$	[%]	$\left[\frac{1}{cm^3}\right]$	[%]	$\left[\frac{1}{cm^3}\right]$
GaAs	Top	114	$1.6{\cdot}10^{31}$	130	$1.8{\cdot}10^{31}$	656	$9.1{\cdot}10^{31}$	772	$1.1{\cdot}10^{32}$
	Centre	122	$4.9{\cdot}10^{30}$	142	$5.7{\cdot}10^{30}$	646	$2.6{\cdot}10^{31}$	717	$2.9{\cdot}10^{31}$
	Bottom	120	$6.2{\cdot}10^{29}$	141	$7.3{\cdot}10^{29}$	632	$3.3{\cdot}10^{30}$	687	$3.6{\cdot}10^{30}$
Si	Top	105	$1.0{\cdot}10^{31}$	117	$1.2{\cdot}10^{31}$	680	$6.7{\cdot}10^{31}$	836	$8.2{\cdot}10^{31}$
	Centre	117	$8.2{\cdot}10^{30}$	130	$9.2{\cdot}10^{30}$	682	$4.8{\cdot}10^{31}$	821	$5.8{\cdot}10^{31}$
	Bottom	122	$2.6{\cdot}10^{30}$	138	$3.0{\cdot}10^{30}$	668	$1.4{\cdot}10^{31}$	777	$1.7{\cdot}10^{31}$

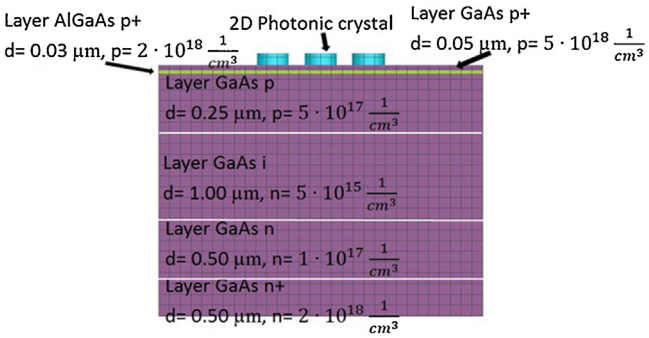

Fig. 21. Parameters of solar cell for possibility PhC's application [45], where: d is the thickness of the layer, p, n are types of doping.

substrate, introduce more radiation inside the structure and allow to generate more carrier.

In the top area of both substrates for PMMA ARC and PhC, we noticed that less of carrier is generated in comparison to ARC and PhC from Al_2O_3. It confirms that the PMMA material absorb the high-energy photons (300–350 nm wavelength, Fig. 8).

2.7. Potential application

One of the possible applications for PhC in optoelectronics is the ARC for photovoltaics. Figure 21 shows an example of the solar cell made of gallium arsenide.

The structure presented in Fig. 21 was simulated with the same set of parameters. The solar cell has been calculated with Lumerical Device CT (Charge Transport). We have calculated the parameters of the solar cell from the standard's setup of Lumerical software [48].

We have compared ARC and PhC again, this time from Al_2O_3's material. The reflectance is the same as in Fig. 3. Furthermore similar construction of the solar cell as an analyzing substrate from GaAs allows the definition of the influence of changing the power density by PhC inside the device on the efficiency of the solar cell.

The deflected effect of PhC increase the efficiency of the solar cell about 6,3% and it is approximately 1% more than for ARC [45].

3. Conclusions and summary

The analysis of photonic crystals as an antireflection coating show that PhC structures have similar parameters of reflectance and transmittance from traditional one-layer ARCs. In the visible range for both analysing substrates, the PhCs made of Al_2O_3 reduces the reflection better than PhCs made by PMMA. Moreover, the comparison of the introduction of power density inside the substrates for PhCs made of different materials shows that PhCs made of Al_2O_3 deflect the radiation better than PhCs made of PMMA. In both cases of Si and GaAs substrates, the difference between the highest value of introducing Poynting vector for PhCs was of 0.3 $\frac{mW}{m^2}$. It confirms that the PhCs, made of material with higher value of refractive index, work better as a new generation ARC.

The differences of the highest value of power density introduced by ARCs and PhCs to the optoelectronic devices are similar for Si and GaAs substrates. However, in Figs. 9 and 11 for PhCs made of Al_2O_3, but deposited on the top of the different substrate, we see that the radiations take similar shape inside the optoelectronic structure (it is a consequence of wave optics), but the quantitatively depends on parameters of substrates material. This quantitatively depends on parameters of substrates material is noticeable in Figs. 13 and 14 as exponentially decays of radiation inside the substrates.

The origins of Poynting vector for only a single wavelength are respondent to the origins of optical generation function. It means that the calculation of Poynting vector for a single wavelength is enough to get information about active area inside the substrate.

This conclusion has got confirmation in the potential application of a new generation coating. The efficiency of the solar cell with PhC as ARCs has approximately 1% more than the solar cell with the traditional ARC.

For best results of the improvement of efficiency of optoelectronic devices, the research of new generation of ARCs has to be investigated.

In summary, we showed the complex optic analysis of a new generation of the ACR. The PhC's structures change the direction of the radiation after passing of that layer. It is not observed on the standard transmission, absorption and reflection characteristics. That characteristics provide only quantitative information about radiation reached the substrate. The complex optic analysis is by Poynting vector inside the optoelectronic device. The energy flow distribution allows helping with construction more effective optoelectronic devices.

Conflict of interest

None.

Acknowledgement

This research was supported by the Statutory Grant of Faculty of Microsystem Electronics and Photonics, Wroclaw University of Science and Technology.

References

[1] A. Macleod, The early days of optical coating, J. Opt. A: Pure Appl. Opt. 1 (1999) 779–783.
[2] U. Sikdera, M.A. Zamanb, Optimization of multilayer antireflection coating for photovoltaic applications, Opt. Laser Technol. 79 (May) (2016) 88–94.
[3] P. Mandal, S. Sharma, Progress in plasmonic solar cell efficiency improvement: a status review, Adv. Mater. Res.—Switzerland 65 (Novemeber) (2016) 537–552.

[4] R. Dewan, M. Marinkovic, R. Noriega, S. Phadke, A. Salleo, D. Knipp, Light trapping in thin-film silicon solar cells with submicron surface texture, Opt. Express 17 (25) (2009) 23058–23065.
[5] J.L. Plawsky, J.K. Kim, E.F. Schubert, Engineered nanoporous and nanostructured films, Mater. Today 12 (June (6)) (2009) 36–45.
[6] K.-S. Han, H. Lee, D. Kim, H. Lee, Fabrication of anti-reflection structure on protective layer of solar cells by hot-embossing method, Solar Energy Mater. Solar Cells 93 (August (8)) (2009) 1214–1217.
[7] P. Bermel, C. Luo, L. Zeng, L.C. Kimerling, J.D. Joannopoulos, Improving thin-film crystalline silicon solar cell efficiencies with photonic crystals, Opt. Express 15 (December (25)) (2007) 16986–17000.
[8] S.J. Fonash, Chapter 3 – Light-trapping structures, in: Light Trapping in Solar Cell and Photo-Detector Devices, Elsevier, 2015, 33–48.
[9] S.-Y. Lin, Experimental Study of Electronic Quantum Interference, Photonic Crystal Cavity, Photonic Band Edge Effects for Optical Amplification, Technical Report, 07 Nov 2014, 11 Jan 2016, New York, 2016.
[10] X. Sheng, L.Z. Broderick, L.C. Kimerling, Photonic crystal structures for light trapping in thin-film Si solar cells: modeling, process and optimizations, Opt. Commun. 314 (March) (2014) 41–47.
[11] P. Chen, G. Hou, H. Qian, Z. Jing, Z. Jianjun, N. Jian, Z. Xiaodan, Z. Ying, F. QiHua, An efficient light trapping scheme based on textured conductive photonic crystal back reflector for performance improvement of amorphous silicon solar cells, Appl. Phys. Lett. 105 (August (7)) (2014), 073506.
[12] A.H. Aly, A.A. Ameen, D. Vigneswaran, Superconductor nanometallic photonic crystals as a novel smart window for low-temperature applications, J. Supercond. Nov. Magn. (2018) 1–7 https://doi.org/10.1007/s10948-018-4716-6.
[13] P. Pathi, A. Peer, R. Biswas, Nano-photonic structures for light trapping in ultra-thin crystalline silicon solar cells, Nanomaterials—Basel 7 (1) (2017) 17.
[14] C. Shemelya, D.F. DeMeo, T.E. Vandervelde, Two dimensional metallic photonic crystals for light trapping and anti-reflective coatings in thermophotovoltaic applications, Appl. Phys. Lett. 104 (January (2)) (2014) 021115.
[15] X.-J. Liu, Y. Liang, J. Ma, S.-Q. Zhang, H. Li, X.-Y. Wu, Y.-H. Wu, Two-dimensional function photonic crystals, Physica E 85 (January) (2017) 227–237.
[16] V. Fakouri-Farid, A. Andalib, Design and simulation of an all optical photonic crystal-based comparator, Optik 172 (2018) 241–248.
[17] Z. Xu, M. Li, M. Xu, J. Zou, H. Tao, L. Wang, J. Peng, Light extraction of flexible OLEDs based on transparent polyimide substrates with 3-D photonic structure, Adv. Polym. Sci. 44 (May) (2017) 225–231.
[18] M. Parchine, T. Kohoutek, M. Bardosova, M.E. Pemble, Large area colloidal photonic crystals for light trapping in flexible organic photovoltaic modules applied using a roll-to-roll Langmuir-Blodgett method, Solar Energy Mater. Solar Cells 185 (October) (2018) 158–165.
[19] S. Baek, et al., Monolithic two-dimensional photonic crystal reflectors for the fabrication of high efficient and highly transparent dye-sensitized solar cells, ACS Appl. Mater. Interface 9 (2017) 37006–37012.
[20] A. Nirmal, et al., Light trapping in inverted organic photovoltaics with nanoimprinted ZnO photonic crystals, IEEE J. Photovolt. 7 (2017) 545–549.
[21] A. Peer, R. Biswas, Nanophotonic organic solar cell architecture for advanced light trapping with dual photonic crystals, ACS Photonics 1 (2014) 840–847.
[22] A.H. Aly, H. Sayed, Photonic band gap materials and monolayer solar cell, Surf. Rev. Lett. 25 (8) (2018) 6, 1850103.
[23] S. Bhattacharya, S. John, Designing high-efficiency thin silicon solar cells using parabolic-pore photonic crystals, Phys. Rev. Appl. 9 (2018) 044009.
[24] J. Joannopoulos, J.N. Winn, S.G. Johns, R.D. Meade, Photonic Crystals: Molding the Flow of Light, Princeton University Press, Princeton, 2008.
[25] J.-M. Lourtioz, H. Benisty, V. Berger, J.-M. Gerard, D. Maystre, A. Tchelnokov, Photonic Crystals: Towards Nanoscale Photonic Devices, Springer, New York, 2008.
[26] P. Nowak, M. Krawczyk, Phononic band gaps in one-dimensional phononic crystals with nanoscale periodic corrugations at interfaces. FDTD and PWM simulations, AIP Conf. Proc. 1 (16) (2010) 85–95.
[27] A.J. Danner, An Introduction to the Plane Wave Expansion Method for Calculating Photonic Crystal Band Diagrams, University of Illinois at Urbana-Champaign, Urbana, 2002.
[28] J.B. Schneider, Understanding the Finite-Difference Time-Domain, January, 2011.
[29] A.D. Polyanin, V.F. Zaitsev, Handbook of Exact Solutions for Ordinary Differential Equations, 2nd edition, Chapman & Hall/CRC, 2002.
[30] J.-M. Liu, Photonic Devices, Cambridge University Press, Cambridge, 2005.
[31] B. Ziętek, Optoelektronika, Toruń: Wydawnictwo Naukowe Uniwersytetu Mikołaja Kopernika, 2005.
[32] M.A. Green, M.E. Watt, R. Corkish, S.R. Wenham, Applied Photovoltaics, Earthscan, 2007.
[33] M.J. Dodge, "Refractive Index" in Handbook of Laser Science and Technology, Volume IV, Optical Materials: Part 2, CRC Press, Boca Raton, 1986.
[34] E. Palik, Handbook of Optical Constants of Solids, Academic Press, 2012.
[35] Lumerical Inc., Lumerical Inc. | Innovative Photonic Design Tools [Online]. Available: http://www.lumerical.com/tcad-products/fdtd/. (Accessed 8 February 2019).
[36] S.G. Johnson, Notes on Perfectly Matched Layers (PMLs), MIT course, 2007.
[37] J.P. Berenger, Perfectly Matched Layer (PML) for Computational Electromagnetics, Morgan & Claypool Publishers, 2007.
[38] S.D. Gedney, B. Zhao, An auxiliary differential equation formulation for the complex-frequency shifted PML, IEEE Trans. Antenn. Propag. 58 (no. 3) (2010) 838–847.
[39] Lumerical Inc., PML Boundary Conditions, [Online]. Available: Lumerical, https://kb.lumerical.com/en/ref_sim_obj_pml_boundary_conditions.html (Accessed 8 February 2019).
[40] V.A. Kuzkin, On angular momentum balance for particle systems with periodic boundary conditions, Zamm-Z Angew. Math. Mech. 95 (11) (2015) 1290–1295.
[41] Lumerical Inc., Bloch Boundary Conditions | Lumerical Knowledge Base, [Online]. Available: Lumerical, https://kb.lumerical.com/en/ref_sim_obj_bloch_bc.html (Accessed 8 February 2019).
[42] H.A. MacLeod, Thin-Film Optical Filters, Institute of Physics Publishing, Bristol, 1986, pp. 2001.
[43] T. Kaino, Y. Katayama, Polymers for optoelectronics, Soc. Plast. E (1989) 1209–1214.
[44] H.M. Zidan, M. Abu-Elnader, Structural and optical properties of pure PMMA and metal chloride-doped PMMA films, Physica B. 355 (1–4) (2005) 308–317.
[45] D. Przybylski, S. Patela, Numerical analysis of the influence of the two dimensional photonic crystals on the efficiency of solar cells, 4th International Conference on Advances in Electronic and Photonic Technologies (2016).
[46] Chapter 25. The measurement of transmission, absorption, emission, and reflection, in: J.M. Palmer, M. Bass (Eds.), Handbook of Optics. Volume II Devices, Measurements, and Properties, McGraw-Hill, Inc., New York, 1995, p. 899.
[47] J.A. Stratton, Electromagnetic Theory, IEEE Press, John Wiley & Sons, New Jersey, 2007.
[48] Lumerical Inc., "Silicon Solar Cell" Lumerical, [Online]. Available: https://apps.lumerical.com/solar_cells_device_getting_started.html. (Accessed 8 February 2019).